ADVANCED ENERGY MATERIALS
www.advenergymat.de

Let It Catch: A Short-Branched Protein for Efficiently Capturing Polysulfides in Lithium–Sulfur Batteries

Min Chen, Chunhui Li, Xuewei Fu, Wei Wei, Xin Fan, Andrew Hattori, Zhiping Chen, Jin Liu,* and Wei-Hong Zhong**

Uncovering the key contributions of molecular details to capture polysulfides is important for applying suitable materials that can effectively restrain the shuttle effect in advanced lithium–sulfur batteries. This is particularly true for natural biomolecules with substantial structural and compositional diversities strongly impacting their functions. Here, natural gelatin and zein proteins are first denatured and then adopted for fabrication of nanocomposite interlayers via functionalization of carbon nanofibers. From the results of experiment and molecular dynamic simulations, it is found that the lengths of the sidechains on the two proteins play critical roles. The short-branched gelatin shows significantly stronger adsorption of polysulfides, as compared with zein comprising many long-chain residues. The gelatin-based interlayer, along with its good porous structures/electrical conductivity, greatly suppresses the shuttle effect and yields exceptional electrochemical performance. Furthermore, the implementation of proteins as functional binder additives further supports the finding that gelatin enables stronger polysulfide-trapping. As a result, high-loading sulfur cathodes (9.4 mg cm^{-2}) are realized, which deliver a high average areal capacity of 8.2 mAh cm^{-2} over 100 cycles at 0.1 A g^{-1}. This work demonstrates the importance of sidechain length in capturing polysulfides and provides a new insight in selecting and design of desired polysulfide-binding molecules.

1. Introduction

Lithium–sulfur (Li–S) batteries with a high theoretical energy density (2600 Wh kg^{-1}[1]) hold great promise to meet the ever-increasing demands for high energy density power supplies. In the meantime, sulfur features natural abundance and non-toxicity, bringing in economic merits for using sulfur as an electrode material. The practical applications of Li–S batteries, however, are still hindered by several issues in both materials and system levels.[2] One of the most critical hurdles is the "shuttle effect" caused by the dissolution/diffusion of electrochemical intermediates of sulfur, lithium polysulfides, in organic liquid electrolytes, and the shuttling of them between the sulfur cathode and lithium anode.[3] The shuttle effect consumes the sulfur active materials and corrodes lithium metal anodes, which degrades the capacity and cycling performance of the batteries.[4] To address this issue, tremendous efforts with the aim of prohibiting the loss/diffusion of sulfur species have been made. One of the conventional strategies is the design of advanced structures of sulfur active materials via encapsulating sulfur in various host materials such as carbon materials (carbon nanofibers,[5] reduced graphene oxide[6] etc.), polymers (polyethylene glycol (PEG),[7] polypyrrole (PPy)[8] etc.) and inorganics (TiO_2,[9] MnO,[10] Al_2O_3[11] etc.). The host materials effectively localize the sulfur species within the sulfur cathode region and suppress their diffusion, which have made great progresses in pushing forward the engineering of Li–S batteries. However, more efforts are needed for improving the fabrication procedures and reducing the costs for mass production.

Compared with architecture design of sulfur active materials, engineering of functional separators or binders represents a cost-effective and scalable strategy. Such approach can not only resolve the shuttle effect, but also be readily adapted with

M. Chen, Dr. C. H. Li, Dr. X. W. Fu, Dr. X. Fan, A. Hattori
School of Mechanical and Materials Engineering
Washington State University
Pullman, WA 99164, USA
E-mail: xuewei.fu@wsu.edu

M. Chen, Dr. Z. P. Chen
College of Materials Science and Engineering
Chongqing University
174 Shezhengjie, Chongqing 400044, China

The ORCID identification number(s) for the author(s) of this article can be found under https://doi.org/10.1002/aenm.201903642.

DOI: 10.1002/aenm.201903642

Dr. W. Wei
Department of Plant Pathology
Washington State University
Pullman, WA 99164, USA

Dr. X. Fan
College of Food Science and Technology and Key Laboratory of Environment Correlative Dietology
Huazhong Agricultural University
No. 1 Shizishan Road, Wuhan 430070, Hubei, China

Prof. J. Liu, Prof. W.-H. Zhong
School of Mechanical and Materials Engineering
Washington State University
Pullman, WA 99164, USA
E-mail: jin.liu2@wsu.edu; katie_zhong@wsu.edu

current battery technologies for widespread implementations. To this end, most of these efforts have focused on employment of functional polar polymers as the polysulfide absorbents, working together with conductive fillers to create separator coatings, such as polyethylene glycol (PEG)-MWCNT,[12] poly(acrylic acid) (PAA)-SWCNT,[13] poly(vinylpyrrolidone) (PVP)-SWCNT[14] etc. Besides, many studies have directly implemented these polar polymers as the binders of sulfur cathodes, such as (poly(ethylene oxide) (PEO),[15] poly(vinylpyrrolidone) (PVP),[16] poly(vinyl alcohol) (PVA),[17] polyethylene imine (PEI)[18] etc. In addition to synthetic polymers, biopolymers that are abundant in nature and aqueously processable recently emerge as a class of intriguing polysulfide immobilizers.[19] Biopolymers have been proved more effective for adsorbing polysulfides due to their vast variety of polar groups (e.g., carboxyl and hydroxyl groups), heteroatom-containing groups (e.g., amine group[20]) and even charged groups,[21] enabling them to show chemisorption/electrostatic interactions of/with polysulfides.[22] Some proteins have been studied as polysulfide absorbents because of the rich functional groups. For example, gelatin protein, was reported for fabricating a conductive separator coating for blocking polysulfides,[21,23] owing to the oxygen-containing groups electrostatically binding with polysulfides. Another type of protein, soy protein[24] was utilized as a blocking layer for polysulfides due to its plentiful amine groups. In addition, various polysaccharides such as gum arabic (GA)[25] and chitosan[26] acting as effective polysulfide trapping agents, were incorporated in separator coatings, due to their abundant oxygen-containing groups or amine groups for chemically adsorbing polysulfides. In addition to the aforementioned applications in separator engineering, more intensive studies have been reported on different proteins such as gelatin,[27] soy protein,[28] γ-polyglutamic acid (PGA)[29] etc. and various polysaccharides such as GA,[30] guar gum (GG),[31] xanthan gum (XG),[32] alginate,[33] Carbonyl-β-Cyclodextrin,[34] sodium carboxyl methyl cellulose (NaCMC),[35] chitosan,[26b] etc. as the functional binders for adsorbing polysulfides and then alleviating the shuttle effect.

The previous efforts have demonstrated the effectiveness of two primary classes of biopolymers, proteins, and polysaccharides, for absorbing the polysulfides in Li–S batteries. The polar groups inside these biopolymer molecules have been believed to be the main reason for binding with polysulfides.[25,28] It is noted that, biopolymers have structural and compositional diversities, which bring about significant impacts on their properties and functions.[36] In spite of great progresses on investigations of specific functional groups that are responsible for adsorbing polysulfides, the important contributions from structures of biopolymers have not been studied. The in-depth understanding of the structural effects on the polysulfide-trapping ability will significantly help identify critical properties/factors for maximizing functions and predict desired biopolymers that will lead to advanced Li–S batteries. This is particularly important considering that a substantial number of biopolymers (proteins or polysaccharides) are still unexplored.

In this study, two proteins, gelatin and zein, are taken as representative examples to investigate the specific contributions of their molecular details to trapping polysulfides via experiments and simulations. These two proteins are first denatured, such that most of the secondary and higher levels of protein structures are destroyed, resulting in random polypeptide chains.[21,37] A significant difference between the two proteins is the length of the sidechain groups. Denatured gelatin is dominated by short sidechains while denatured zein is mainly composed of long sidechains. We design and fabricate advanced protein-based interlayers via surface functionalization of carbon nanofibers (CNFs) by the denatured proteins. Our results show that the length of the sidechains, play a critical role in trapping the polysulfides. In specific, the short-branched gelatin protein shows tremendously greater adsorption of polysulfides compared with zein protein. As a result, the batteries with gelatin-based interlayer show much better and excellent electrochemical performance. Furthermore, gelatin is also adopted as an advanced binder additive for realization of high-loading sulfur cathodes owing to the great polysulfide-capturing ability.

2. Results and Discussion

2.1. Fabrication and Properties of Protein-Based Interlayers

To investigate the effects of the spatial molecular structures on polysulfide-trapping, two types of proteins, gelatin and zein with significantly different structures, are adopted for fabrication of conductive interlayers for capturing polysulfides (**Figure 1**a–c). Both proteins have been denatured first in a solvent mixture of acetic acid (AA) and distilled water (DI) with a weight ratio of 8:2. The denaturation process effectively breaks the H-bonds and salt-bridges, destroys most of the secondary and higher levels of the molecular structures, and results in random polypeptide chains with different side groups.[37,38] This process is necessary to expose the functional groups that are hidden in the native protein for interacting with other components. The protein-functionalized interlayers are fabricated via growing of thin protein coatings on the surface of carbon nanofibers. This process leads to networked fibrous structures with CNFs as the conductive backbones and protein coatings as the active polysulfide binding sites. More fabrication details can be found in the Experimental Section (Supporting Information). The gelatin-based interlayer shows remarkable adsorption of polysulfides compared with the zein-based interlayer in Figure 1b,c. Since the active polysulfide binding sites come mainly from the charged oxygen atoms on the protein backbones (see Section 2.3), the main difference in the absorption function stems from the specific molecular structures (length of sidechains) of the two proteins. As depicted in Figure 1d,e, zein primarily comprises amino acids with long chains, such as glutamic acid (Glu), leucine (Leu), and phenylalanine (Phe). In contrast, gelatin possesses more simple chain structures and mostly consists of short-chain amino acids, e.g., glycine (Gly), proline (Pro), and alanine (Ala). As a result, the long sidechains of zein severely block the access of active sites at protein backbones for trapping polysulfides, as demonstrated in Figure 1f. For gelatin, however, the simple protein configuration and short sidechains do not block the polysulfides and make the active adsorbing sites easily accessible, as illustrated in Figure 1g. The details will be discussed in the following sections through experiments and simulations. It should be noted that with the introduction of an interlayer, the

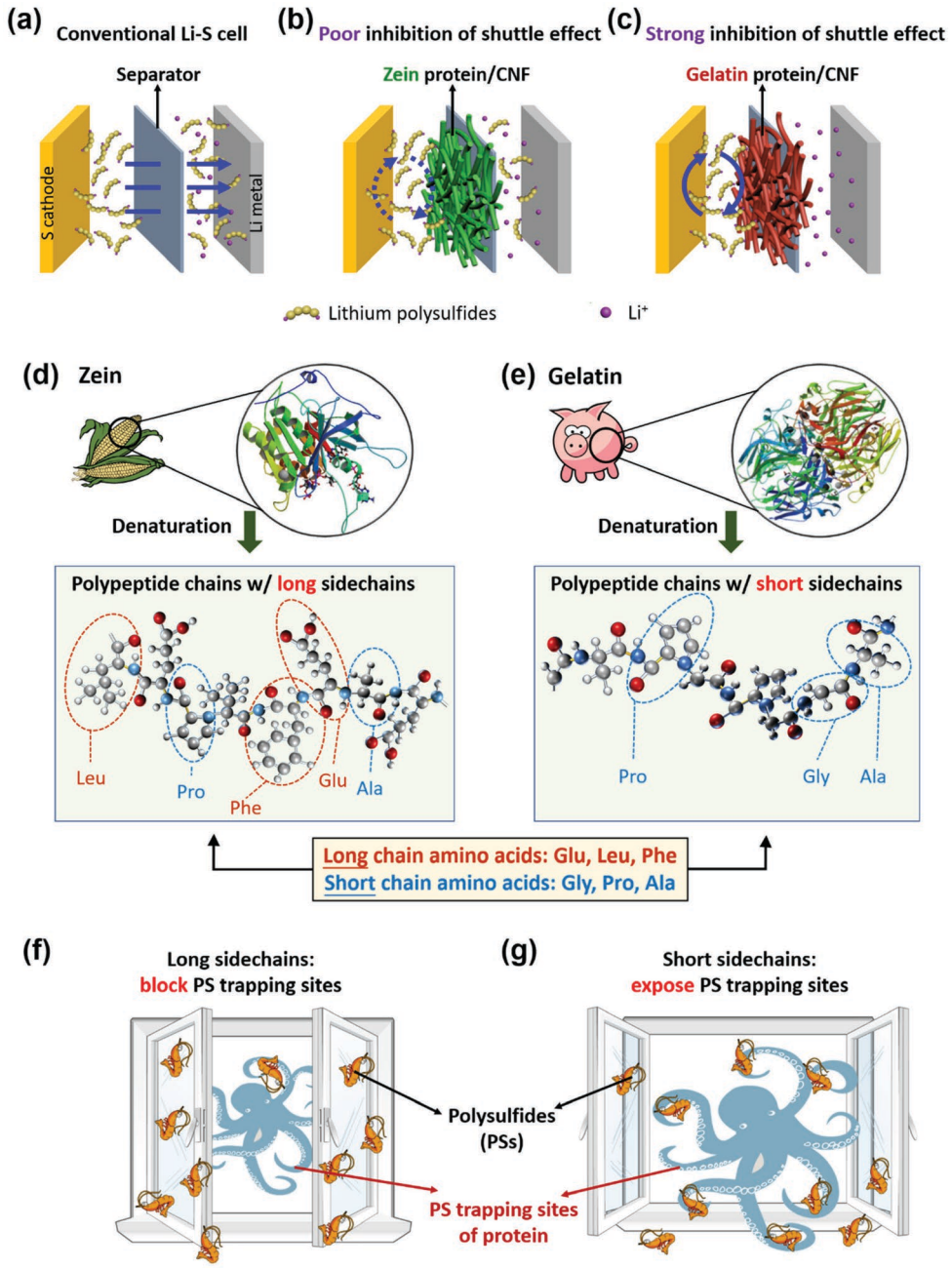

Figure 1. Schematic illustration of the design strategy and effects of protein structures on capturing polysulfides. Schematics of the shuttle effect in different Li–S batteries with a) pristine separator and with different protein-functionalized interlayers: b) zein/CNF and c) gelatin/CNF interlayers. Schematics of the denaturation process and typical polypeptide chains of d) zein protein mainly consisting of long sidechains, and e) gelatin protein mainly consisting of many short sidechains. Illustrations of the effects of proteins' sidechain groups on polysulfide-trapping ability: f) long sidechain groups of zein protein block the polysulfide trapping sites; g) short sidechain groups of gelatin protein expose the polysulfide trapping sites.

energy density of the battery is inevitably decreased. Therefore, toward practical applications, it is in an urgent need to further optimize the structure design and fabrication process to make the interlayers as thin and as light as possible.

The amino acids, as the building blocks of proteins, are first investigated by amino acid analyzer and the results are shown in **Figure 2**a (the complete amino acid profiles can be found in Table S1, Supporting Information). As shown, the two proteins have significantly different amino acid profiles. The dominant amino acids are Glutamic acid (Glu, 23.6 wt%) and Leucine (Leu, 17.5 wt%) for zein, and are Glycine (Gly, 23.5 wt%) and Proline (Pro, 15.2 wt%) for gelatin. From the structures of the amino acids shown in Figure 2a, it can be clearly seen that both Glu and Leu possess much longer backbone chains, while Gly and Pro show much simpler chain structures and shorter backbones. These different amine acids lead to different sidechain

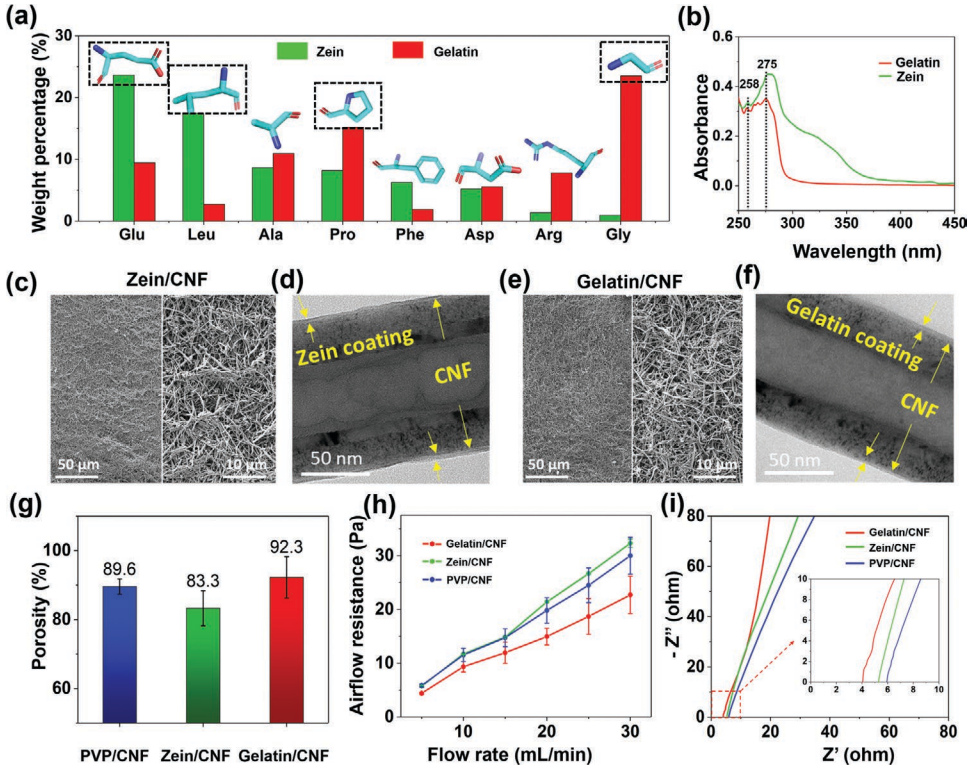

Figure 2. Compositions of proteins, morphological and ionic conductivity studies of different interlayers. a) Weight percentage of primary amino acids of zein and gelatin. b) UV–vis spectra of zein and gelatin solutions (dissolved in acetic acid aqueous solvents (pH = 2)). c,d) SEM and TEM images of zein/CNF nanocomposite, respectively. e,f) SEM and TEM images of gelatin/CNF nanocomposite, respectively. g) Porosity of various nanocomposite interlayers. h) Air flow resistance (pressure drop) versus varying flow rates of various nanocomposite interlayers. i) Nyquist plots of various nanocomposite interlayers tested in stainless steel/separator/stainless steel configurations.

structures of the two proteins, contributing to the different polysulfide-trapping capability, which will be discussed in detail later. The UV–vis spectra in Figure 2b also indicate the presence of several typical amino acids containing aromatic ring structures that absorb UV light. For both proteins, the distinct peaks at around 275 and 258 nm correspond to Tyrosine (Tyr) and Phenylalanine (Phe), respectively.[39] For zein protein, the absorption peaks at 280 nm and the broad band between 300 and 350 nm may be assigned to Tryptophan (Try).[40]

The protein/CNF nanocomposite interlayers are fabricated via coating of proteins on CNF surface. For comparison, a conventional nanocomposite interlayer composed of a synthetic polymer (PVP) and CNFs is also fabricated, since PVP has demonstrated strong chemisorption to polysulfides.[41] As shown in Figure 2c–f (also see SEM images of PVP/CNF in Figure S1, Supporting Information), the CNFs are randomly interconnected for three types of nanocomposites, which leads to highly porous networked structures in favor of the infiltration of liquid electrolytes. As shown in Figure S2 (Supporting Information), the thickness of the three nanocomposite interlayers (indicated by the cross-sectional SEM images), is kept consistent as ≈15 μm. The contact angles of liquid electrolytes are all decreased from 71° for the pristine separator to less than 12° for the three types of nanocomposite interlayers (Figure S3, Supporting Information). The TEM images (Figure 2d,f) demonstrate that zein and gelatin are successfully grown on the CNFs surface, forming a very thin protein layer (≈4 nm) (see the TEM images of pure CNFs in Figure S4, Supporting Information). This is realized via strong interactions between proteins and CNFs due to the hydrophobic interactions (e.g., π–π interaction) between the aromatic residues of proteins and the CNF surface.[42]

Good porous structures of the interlayers are beneficial for promoting the transport of Li^+ ions and reducing the cell resistance. As the three types of CNF-nanocomposites show similar microstructures, we first measured the porosity of the nanocomposites in Figure 2g. It is found that the interconnected architecture of CNFs gives rise to high porosities for three nanocomposites. Specifically, gelatin/CNF exhibits the highest porosity of 92.3%, and PVP/CNF shows a slightly higher porosity of 89.6% than that of zein/CNF (83.3%). As the pores of the nanocomposites are not regularly shaped, to further understand the effects of pore structures on ion-transport kinetics, we measured the airflow resistance of the nanocomposite interlayers. It is well known that the airflow resistance is highly dependent on the pore structures of the nanocomposites. A lower airflow resistance generally indicates a better spatial pore distribution and a higher porosity,[43] which qualitatively reflects the porous structures that strongly impact the ion-transport resistance. As shown in Figure 2h, the airflow resistances of the gelatin/CNF interlayer are obviously lower than that of PVP/CNF and zein/CNF interlayers at all flow rates. At the same time, one finds that the higher flow rate leads to a more evident increase of airflow resistance,

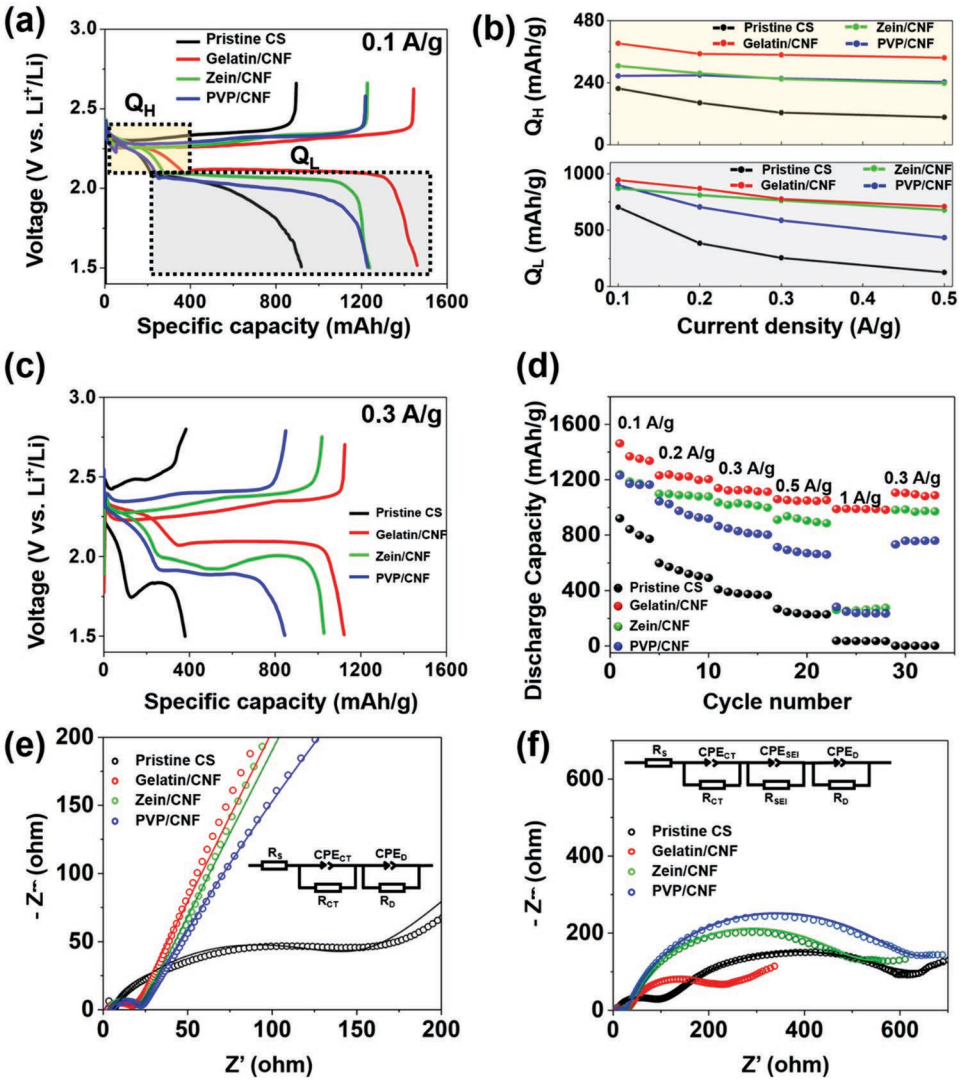

Figure 3. Electrochemical performances of Li-S batteries with different interlayers as compared with the pristine separator. a) Initial charge-discharge profiles at a current density of 0.1 A g^{-1}. b) Capacity fading of the upper and lower discharge plateaus (Q_H and Q_L, respectively) at varying current densities. c) Charge-discharge profiles at a medium current density of 0.3 A g^{-1}. d) Rate performance comparison at varying current densities. Nyquist plots of discharged cells e) before and f) after 10 cycles at a current density of 0.3 A g^{-1} over a frequency range of 0.01–1 MHz. The solid lines indicate the fitting results.

resulting from the more sensitive reflection of the porous structures. The results indicate that gelatin/CNF shows the best porous structure, which helps reduce the ion-transport resistance introduced by the additional interlayers. The ion-transport resistance of the various interlayers is compared in Figure 2i. It is found that the gelatin/CNF interlayer exhibits the lowest ion-transport resistance of 4.1 Ω, compared with the zein/CNF (5.3 Ω) and PVP/CNF (5.9 Ω) interlayers. The inconsistence between the ion-transport resistance and air-flow resistance of zein/CNF and PVP/CNF arises from the unique surface properties of zein. As zein possesses abundant functional groups, which may show unique interactions with ions thus helping the ion-transport.[28,44] The optimal porous structure and low ion-transport resistance of gelatin/CNF interlayer will significantly benefit the battery performance especially the rate capability.

2.2. Electrochemical Performance of Interlayers

The electrochemical performances of Li–S cells with different nanocomposite interlayers are compared with commercial separators. As shown in **Figure 3**a, the cells equipped with nanocomposite interlayers show much higher initial capacity than that of the cell with a commercial separator (capacity of 918 mAh g^{-1}). Interestingly, for the two protein/CNF interlayers, gelatin/CNF cell shows a much higher capacity of 1460 mAh g^{-1} than that of the zein/CNF cell (1239 mAh g^{-1}). The PVP/CNF cell presents a capacity of 1230 mAh g^{-1}, which is similar with the zein/CNF cell but much lower than that of the gelatin/CNF cell. These results suggest that the CNF nanocomposite interlayers effectively suppress the diffusion of polysulfides and the loss of sulfur active materials. Importantly, the gelatin/CNF interlayer shows the strongest polysulfide-trapping

ability, which leads to the greatest utilization of sulfur active materials (87.2%) and the highest capacity.

To further explore the insight of the interlayers on suppressing the shuttle effect, we analyzed the voltage profiles of the cells. It is known that the two distinct discharge voltage plateaus in the four cells represent the redox reactions that are the characteristics of Li–S batteries. The upper discharge plateau is relevant to the conversion of cyclo-S_8 to soluble long-chain polysulfides (Li_2S_n, $4 \le n \le 8$) and the lower plateau is attributed to the further reduction of long-chain polysulfides to insoluble sulfides of Li_2S_n ($n = 1, 2$).[45] Therefore, tracking the change of capacity for both stages is important for understanding of the loss of sulfur species and redox reactions.[25] The capacities of the upper and lower voltage plateaus are extracted from the discharge voltage profiles in Figure 3a and denoted as Q_H and Q_L, respectively. As shown in Figure 3b. The cell with the gelatin/CNF interlayer yields the highest Q_H values among the three types of nanocomposite interlayers at all current densities, while the Q_H values of cell with the commercial separator are the lowest. These results demonstrate that the shuttling of polysulfides is greatly suppressed by the nanocomposite interlayers, especially the gelatin/CNF interlayer. For Q_L, the two protein/CNF interlayers (gelatin/CNF and zein/CNF interlayers) show much slower capacity fading against increased current densities, compared with the cells with the PVP/CNF interlayer and a commercial separator. This implies that the two types of protein/CNF interlayers have stronger ability to capture polysulfides and allow sufficient redox reactions of polysulfides; more interestingly, the gelatin/CNF interlayer shows higher effectiveness than that of the zein/CNF interlayer.

At an elevated current density of 0.3 A g^{-1} (Figure 3c), the capacities of all cells are decreased. However, the gelatin/CNF cell still outperforms the other three cells. It is noted that the voltage platform of the gelatin/CNF cell appears at 2.1 V, which almost stays unchanged compared with the case at 0.1 A g^{-1}. On the other hand, the cells with the zein/CNF and PVP/CNF interlayers as well as a pristine separator show severe polarization, displaying unstable voltage plateaus and much increased voltage hysteresis. The smallest voltage hysteresis and smooth voltage profile of the gelatin/CNF cell indicate that the gelatin/CNF interlayer enables effective polysulfide-trapping and fast redox kinetics simultaneously. These results indicate two key points. First, the good porous structures of the gelatin/CNF interlayer as discussed above significantly reduce the ion-transport resistance, and thus ensure smooth redox reactions and small voltage hysteresis. Second, the gelatin/CNF interlayer more effectively captures and converts the trapped polysulfides, although two kinds of proteins show stronger adsorption of polysulfides and lead to higher capacities than the PVP/CNF interlayer, which will be discussed in detail later.

To further study the advantages of the gelatin/CNF interlayer on the battery performance, we tested the rate performance of different interlayers in comparison of the pristine separator. Figure 3d plots the specific discharge capacities versus different current densities. The cell with a pristine separator shows a poor rate performance. It yields average discharge capacities of 832, 539, 382, 239, and 35 mAh g^{-1} at the current densities of 0.1, 0.2, 0.3, 0.5, and 1 A g^{-1}, respectively, and fails to recover after the current density is changed back to 0.3 A g^{-1}. However, an evident improvement in the rate performance is achieved by the three nanocomposite interlayers. As shown, among the three interlayers, the gelatin/CNF interlayer delivers the highest capacities throughout all the current densities, followed by the zein/CNF and PVP/CNF interlayers. More importantly, at a high current density of 1 A g^{-1}, the capacity of the gelatin/CNF cell (987 mAh g^{-1}) is even about four times as high as the corresponding capacities of the zein/CNF and PVP/CNF cells (262 and 246 mAh g^{-1}, respectively). Meanwhile, the capacity retention of the gelatin/CNF cell (95.7%) is the highest, compared with the zein/CNF (84.2%) and PVP/CNF (80.5%) interlayers, when switching the current densities from 1 to 0.3 A g^{-1}. The exceptional rate performance of the gelatin/CNF cell is the combined result of good porous structures and effective capturing of polysulfides, which leads to fast ion-transport, reduced loss of sulfur species, and smooth polysulfide-conversion kinetics.

Electrochemical impedance spectroscopy (EIS) was conducted on the cells before and after cycling for understanding of the electrochemical reaction kinetics. Typical Nyquist plots with equivalent circuit models are illustrated in Figure 3e,f and the electrochemical impedance parameters are summarized in Table S2 (Supporting Information). The intercepts of the plots on the real axis at high frequency are related to the bulk resistance (R_b). For the cells before cycling, the Nyquist plots are composed of a single semicircle (charge-transfer resistance, R_{CT}) and an inclined line (diffusion process, R_D[46]). During the electrochemical reaction of sulfur reduction, the CNF interlayers trap the dissolved polysulfides, transfer electrons to them and convert them into Li_2S/Li_2S_2. Therefore, as shown, R_{CT} value of the cell with a pristine separator (132.2 Ω) is much higher than that of the cells with the nanocomposite interlayers (18.7, 18.3, and 14.4 Ω for zein/CNF, PVP/CNF, and gelatin/CNF interlayers, respectively), which is ascribed to the improved electrical conductivity (see the electrical conductivity results of the interlayers in Figure S5, Supporting Information) and enlarged conductive surface area by the nanocomposite interlayers.

After cycling, the Nyquist plots consist of two sequential semicircles at high-to-medium frequency region. The first semicircle represents the charge-transfer resistance, and the second one at middle frequency region corresponds to interface impedance (R_{SEI}), which indicates lithium ion diffusion resistance through the Li_2S/Li_2S_2 solid film.[47] At low frequency region there are also diffusion-related inclined lines. Interestingly, the cell with the pristine separator show decreased R_{CT} values, which may be ascribed to the improved interfacial wettability and lithium ion diffusion with cycling. The other three cells show slightly increased R_{CT} values which are mainly due to the morphology change of the electrodes and the interlayers, and the deposited sulfur species during cycling. In addition, the gelatin/CNF cell shows the lowest value of R_{SEI} (114.6 Ω), while the R_{SEI} values of zein/CNF (401.9 Ω) and PVP/CNF (507.2 Ω) cells are much higher. This indicates that the gelatin/CNF interlayer enables the most effective absorption of polysulfides, and therefore prohibits their diffusion to lithium metal anodes.

The cycling performance of the nanocomposite interlayers was first evaluated at a medium current density of 0.3 A g^{-1}. As shown in **Figure 4**a, the cells with the three kinds of interlayers

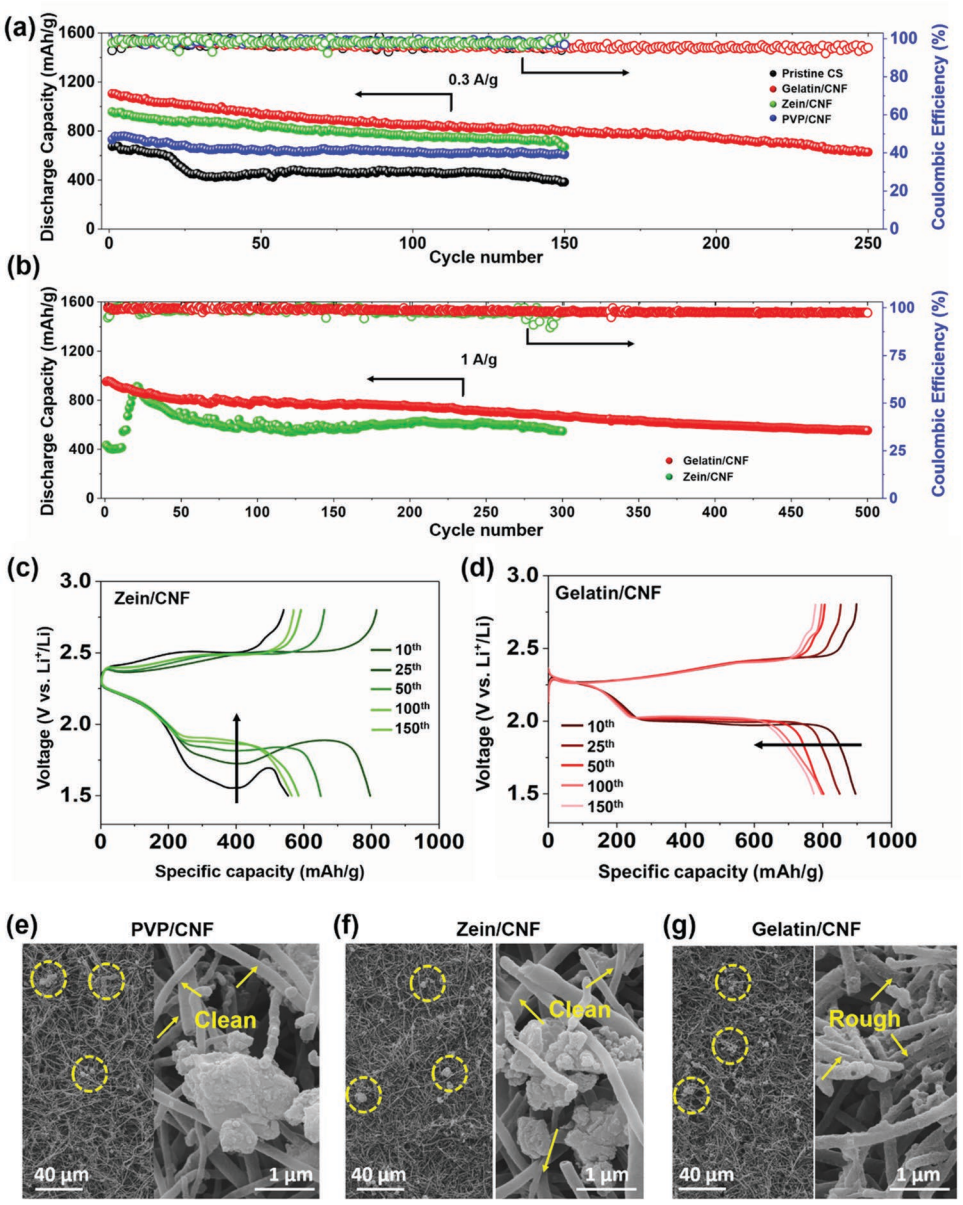

Figure 4. Electrochemical performances of Li–S batteries with two types of protein/CNF interlayers. Cycle stability and Coulombic efficiency at a current density of a) 0.3 A g^{-1} and b) 1 A g^{-1}. Charge–discharge profiles upon various cycle numbers of Li–S batteries with c) zein/CNF and d) gelatin-CNF interlayers at a current density of 1 A g^{-1}. SEM images of e) PVP/CNF, f) zein/CNF, and g) gelatin/CNF interlayers after C-rate testing at discharging state.

show much higher capacities and better long-term stability, compared with the cell with a pristine separator. Specifically, the pristine separator cell yields an initial discharge capacity of 674 mAh g^{-1} and the capacity drastically decays upon about 25 cycles, due to a substantial loss of sulfur active materials and the severe shuttle effect. After 150 cycles, the retention capacity is only 384 mAh g^{-1}. The initial discharge capacities are significantly improved to 1105, 957, and 731 mAh g^{-1} by gelatin/CNF, zein/CNF and PVP/CNF interlayers, respectively. Meanwhile, the two protein/CNF interlayers keep their advantages over the PVP/CNF interlayer, and demonstrate much higher capacities during the cycling testing than that of the PVP/CNF cell. More significantly, the gelatin/CNF cell presents the highest capacities throughout the tested cycles, the retention capacity of which is 628 mAh g^{-1} after 250 cycles. To fully elucidate the contributions from different proteins on electrochemical performance, we further studied the cycling stability of the cells armed with two types of protein/CNF interlayers at a high current density of 1 A g^{-1}. As shown in Figure 4b, the cell with the gelatin/CNF interlayer exhibits higher capacities and better cycling stability than that of the zein/CNF interlayer. The initial capacities of gelatin/CNF cell and zein/CNF cell are 957 and 434 mAh g^{-1}, respectively. However, we find that the zein/CNF cell undergoes an obvious activation process in the first several cycles and the capacity gradually increases to 913 mAh g^{-1} after 25 cycles. Subsequently, the capacity noticeably fades and falls to 548 mAh g^{-1}

after 300 cycles, with an average Coulombic efficiency of 94.4% and a capacity decay rate of 0.14% per cycle. In contrast, the gelatin/CNF cell shows much stable cycling performance with a much higher average Coulombic efficiency (99.0%). In addition, even after 500 cycles, the gelatin/CNF cell remains a capacity of 553 mAh g^{-1} with a decay rate of only 0.084% per cycle. The results clearly identify that the gelatin/CNF interlayer more effectively suppresses the shuttling behavior of polysulfides and ensures sufficient redox reactions. The charge-discharge profiles of cells with the zein/CNF and gelatin/CNF interlayers upon certain cycle numbers are illustrated in Figure 4c,d. As shown in Figure 4c, from the 10th to the 50th cycle, the polarization phenomenon of the zein/CNF cell gradually weakens with an increase of the capacity, and then the capacity fades from the 50th to 250th cycle. However, the gelatin/CNF cell exhibits smooth voltage profiles with stable voltage hysteresis during cycling processes in Figure 4d. This comparison implies that the gelatin/CNF interlayer performs much better in refraining the shuttle effect and providing fast redox reactions.

The above electrochemical performance studies indicate two important points: 1) proteins (gelatin and zein) show stronger adsorption of polysulfides compared with conventional polymers (e.g., PVP); 2) gelatin demonstrates higher polysulfide-trapping ability than zein. To investigate how the nanocomposite interlayers contribute to capturing polysulfides, we examine the morphologies of the interlayers after cycling testing. As shown in Figure 4e–g, all interlayers can trap the polysulfides as indicated by the accumulated big sulfur-related particles deposited on the nanocomposites. However, if we take a closer look, significantly different morphologies are observed (More SEM images in Figure S6, Supporting Information). For PVP/CNF and zein/CNF interlayers, we find that the surface of CNFs is clean and smooth without growth of trapped polysulfides, indicating poor interactions between PVP/zein and polysulfides. Therefore, the polysulfides are trapped mainly due to the size exclusion effect. This can be further proved by the fact that sulfur species accumulates to form big particles at the intersections of the CNFs. Nonetheless, the big sulfur-related particles may seriously block the pathways for transport of Li^+ ions. At the same time, due to the poor adsorption of polysulfides by the interlayers, e.g., zein/CNF, the transformation of polysulfides are controlled by a diffusion process as illustrated in Figure S7a (Supporting Information). These two factors result in the severe polarization of the zein/CNF cell as shown in Figure 4c. On the other hand, polysulfides are notably captured by each individual carbon nanofiber of the gelatin/CNF interlayer, as indicated by the rough surface of CNFs (Figure 4g). This implies that the functional gelatin coating on the CNF surface gives rise to a much stronger polysulfide-trapping ability than zein and PVP, leading to a uniform absorption of polysulfides throughout the carbon fibers. The EDS mappings of the cycled gelatin/CNF interlayer in Figure S8 (Supporting Information) show that there is a strong signal from sulfur element on both the fiber surface and the large particles, which verifies that the gelatin/CNF interlayer can strongly trap polysulfides. The mechanistic illustration in Figure S7b (Supporting Information) indicates that the conversion of polysulfides in-situ occur on the fiber surface of the gelatin/CNF interlayer, which yields very smooth redox reactions in long-term cycling (Figure 4d).

2.3. Simulation Studies of Proteins for Catching Polysulfides

To gain in-depth insights into the fundamental mechanisms, we performed molecular dynamic (MD) simulations on absorption of polysulfides by the two proteins after denaturation: gelatin and zein (simulation details, Supporting Information). **Figure 5**a,b illustrates the snapshots of the initial and final (at 200 ns) states of the adsorption process of Li_2S_4 by proteins. As shown in initial states, both gelatin and zein are surrounded by the same number of polysulfide molecules. After 200 ns, almost all polysulfides are absorbed by gelatin that acts as a spatial "molecular cage" entrapping the polysulfides in Figure 5a; in contrast, zein only adsorbs a small amount of polysulfides (Figure 5b). The simulation data indicate that the most significant polysulfide-binding sites are the backbone and negatively charged oxygen atoms (Li–O interactions). The nitrogen atoms on the backbone are also negatively charged, but the attractions with Li are weaker compared with backbone oxygen atoms due to the less amount of charge and spatial arrangement. The attractions from the sidechains are weak because of the smaller number of binding sites compared with backbone oxygen atoms, but the chain structure (length) significantly impacts the ability of trapping polysulfides. Specifically, gelatin has simple chain structures, mainly consisting of short-chain residues (Gly, Pro, etc.) as illustrated by Figure 2a. The unique chain structures of gelatin effectively open up the protein backbones and expose the backbone oxygens for capturing polysulfides, making the gelatin an excellent polysulfide-trapping cage. Meanwhile, it is also found that the oxygen atoms from the end groups (COO^-) can capture polysulfides because of the electrostatic interactions. However, the oxygen atoms that can adsorb polysulfides are greatly inhibited in the case of zein. As shown in Figure 5b, throughout the simulation process, zein shows extremely weak ability to trap polysulfides and the overall interactions between zein and polysulfides are very unstable. Recall in Figure 2a that zein comprises a large number of long-chain residues (Glu, Leu, etc.). The long-chain residues block the backbone oxygens for trapping polysulfides. At the same time, the access of polysulfides into the protein molecules is even inhibited by the long-chain residues. As a result, only the end group oxygen atoms can adsorb polysulfides. According to the amino acid compositions, oxygen contents of gelatin and zein are estimated to be 21.7 and 22.7 wt%, respectively. Although zein has comparable number of oxygen atoms with gelatin, most of them are "inactive sites" that are separated by long-chain residues and are unable to absorb polysulfides. From the detailed analysis of the interactions between proteins and polysulfides (Figure 5c–e), it is clear that gelatin can trap more polysulfides (Figure 5c) and shows much stronger interactions, such as higher electrostatic force in Figure 5d and higher van der Waals force in Figure 5e with polysulfides, as compared with zein. To testify our findings, another type of protein with completely different amino acid compositions, that is, soy protein (SP), is denatured and then utilized to fabricate the nanocomposite interlayer. Soy protein mainly consists of Glu (17.1%), Asp (10.1%), Leu (6.3%), Arg (6.2%), etc. (Table S1, Supporting Information), which are all long-chain amino acids. Therefore, among the three proteins: gelatin, zein and soy protein, gelatin has the simplest chain structures and

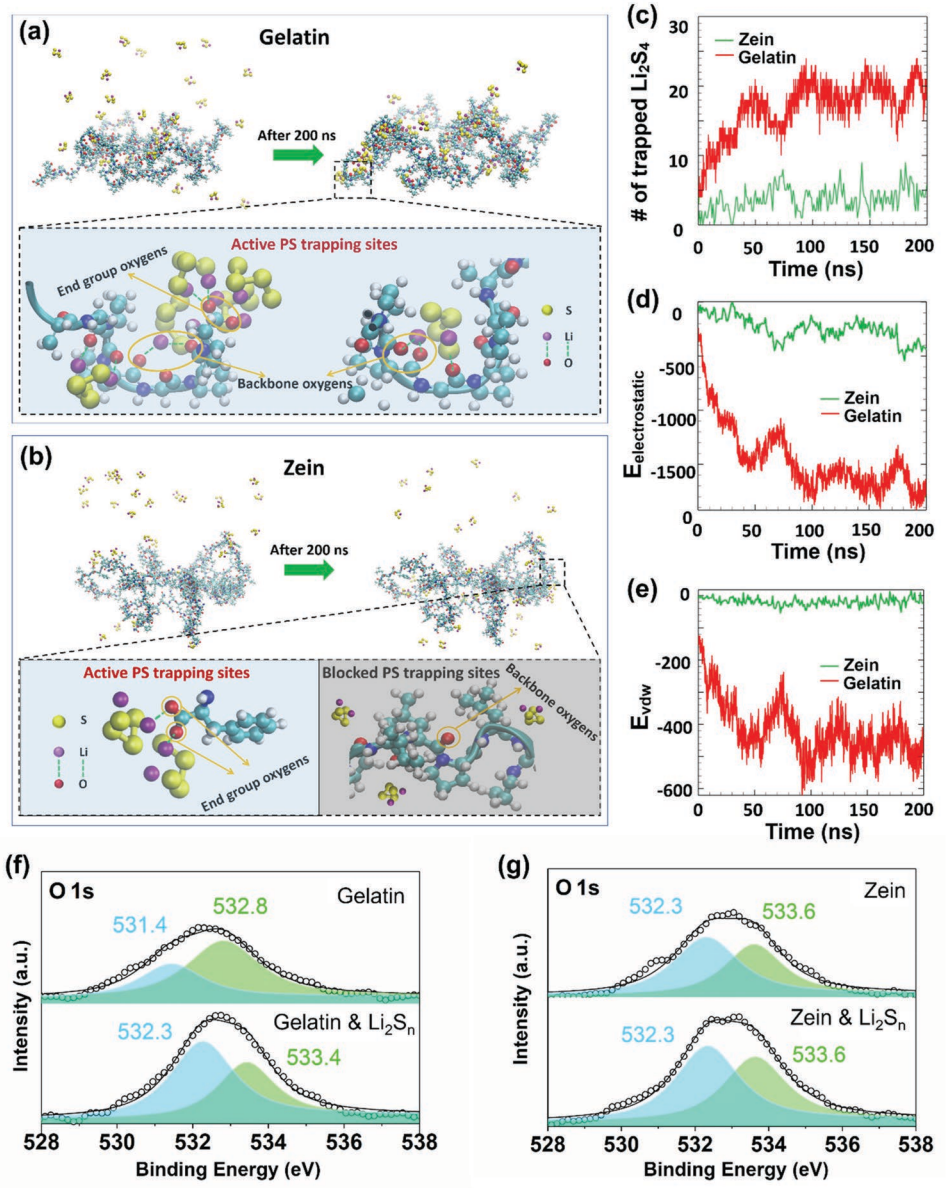

Figure 5. Mechanism studies of the interactions between proteins and polysulfides. Snapshots of the initial and final states of interactions between Li_2S_4 and a) zein and b) gelatin. c) Number of trapped Li_2S_4 by proteins verses time. d) Electrostatic forces between Li_2S_4 and proteins. e) Van der Waals forces between Li_2S_4 and proteins. Deconvoluted O 1s XPS spectra of f) gelatin/CNF interlayer and g) zein/CNF interlayer before and after immersion in 1×10^{-3} M Li_2Sn solution.

is dominated by short sidechains. Introducing the three types of protein-based interlayers in Li–S batteries, the battery with gelatin/CNF interlayer delivers the highest capacity (Figure S9, Supporting Information), which indicates that gelatin shows the strongest polysulfide-trapping capability. This is consistent with our finding that short sidechains play an important role in trapping polysulfides.

X-ray photoelectron spectroscopy (XPS) analysis is carried out to verify the interactions between proteins and polysulfides. As shown in Figure 5f,g, the O 1s spectrum can be deconvoluted into two peaks (wide-scan survey spectra can be found in Figure S10, Supporting Information). The peak with lower binding energy is ascribed to oxygen forming double bonds with carbon (including O—C=O and O=C—N) and the peak with higher binding energy corresponds to oxygen that is single bonded with hydrogen or carbon (C—OH and C—O—C).[48] For the gelatin sample (Figure 5f), the two distinct peaks that are originally at 531.4 and 532.8 eV shift to 532.3 and 533.4 eV, respectively, after immersion in polysulfide solutions. This indicates a notable interaction between oxygen atoms of gelatin and polysulfides. However, no significant peak shift is observed for the case of zein in Figure 5g, suggesting weak interactions between zein and polysulfides. The results are consistent with the simulation data.

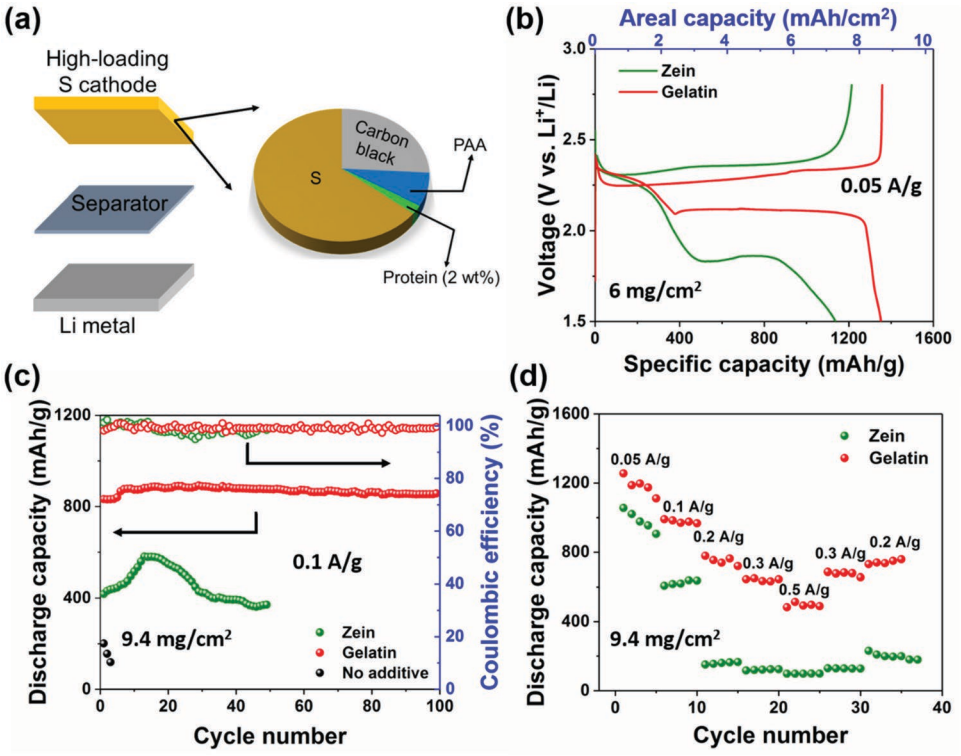

Figure 6. Electrochemical performances of high-loading sulfur cathodes with proteins as the functional additives. a) Compositions of high-loading sulfur cathodes with proteins as functional additives. b) Charge–discharge profiles of 6 mg cm^{-2} sulfur loading cathodes at 0.05 A g^{-1}. c) Cycling stability of 9.4 mg cm^{-2} sulfur loading cathodes at 0.1 A g^{-1}. d) Rate performance of 9.4 mg cm^{-2} sulfur loading cathodes.

2.4. Proteins as Functional Binder Additives

The above studies have analyzed the important contributions from proteins' molecular structures to trapping polysulfides. The results show that gelatin is more advantageous over zein, regarding the adoption of the proteins as polysulfide trapping agents in interlayers. To demonstrate the universality of the finding that the short-branched gelatin performs better than the long-branched zein in capturing polysulfides, we add a small portion of proteins (accounting for 20 wt% in the binder and 2 wt% in the cathode) as the binder additives and polysulfide trapping agents to the sulfur cathodes (**Figure 6**a). As shown in Figure 6b, for the cathodes with a high sulfur loading of 6 mg cm^{-2}, the discharge capacity of the gelatin-cathode (1348 mAh g^{-1}) is much higher than that of the zein-cathode (1137 mAh g^{-1}). The corresponding areal capacities are as high as 8.1 and 6.8 mAh cm^{-2} for the gelatin-cathode and zein-cathode, respectively, which significantly exceed the commercial Li-ion batteries (≈4 mAh cm^{-2}). This result indicates that gelatin more effectively attracts the polysulfides and improves the utilization of sulfur active materials. Interestingly, the functional protein additives enable the realization of a further increase of the sulfur loading to 9.4 mg cm^{-2}. It is found in Figure 6c that, compared with the additive-free cathode failing to deliver stable capacities, the gelatin-cathode yields an excellent cycling stability compared with the zein-cathode that shows a dramatic capacity fading. In specific, the gelatin-cathode presents a stable and remarkable average capacity of 869 mAh g^{-1} (areal capacity: 8.2 mAh cm^{-2}) and a high Coulombic efficiency of 99.2%, compared with the zein-cathode (Coulombic efficiency: 98.5%). This indicates that the shuttle effect is significantly reduced by the gelatin additive compared with zein. In addition, at different current densities (Figure 6d) the gelatin-cathode shows substantially higher capacities than that of the zein-cathode, in particular, at current densities of 0.2–0.5 A g^{-1}. The above results demonstrate that adding the short-branched gelatin molecules into a Li–S battery, e.g., into an interlayer or a sulfur cathode, effectively restrains the shuttle effect owing to the unique molecular structures that bring about strong adsorption of polysulfides.

3. Conclusions

We report a systematic study on revealing the significant contributions of molecular details of proteins to capturing polysulfides and identifying desired structures leading to the exceptional polysulfide-trapping ability. Surface functionalization of CNFs is obtained by applying denatured gelatin and zein. The resulting protein-based nanocomposite interlayers for effectively blocking/adsorbing the polysulfides are fabricated. Our experimental and simulation results demonstrate that short-branched gelatin has notably stronger adsorption of polysulfides compared to that with zein mainly consisting of long sidechains. Molecular dynamic simulation results show that the primary binding sites for polysulfides are the negatively charged oxygens on the backbone; short-chain residues open up the binding sites on protein backbones and allow the

access of polysulfides into the protein "molecular cage", while the long-chain residues block the protein-polysulfide interactions. As a result, together with the good porous structures/electrical conductivity, the gelatin-based interlayer more effectively suppresses the shuttle effect and demonstrates remarkable electrochemical performance (discharge capacity of 553 mAh g^{-1} after 500 cycles at 1 A g^{-1}). Study of proteins as functional binder additives further supports the finding that gelatin enables higher effectiveness for trapping polysulfides. Benefiting from the strong polysulfide-capturing capability of gelatin, high-loading sulfur cathodes (9.4 mg cm^{-2}) show stable cycling performance with an excellent average areal capacity of 8.2 mAh cm^{-2}. This study uncovers the significance of denatured protein structures on trapping polysulfides and provides a guideline for the selection and design of favorable molecules for advanced Li–S batteries.

Supporting Information

Supporting Information is available from the Wiley Online Library or from the author.

Acknowledgements

This work was partially supported by NSF CBET 1604211 and 1929236. M.C. and X.F. were sponsored by the China Scholarship Council. The authors would like to gratefully acknowledge the support on microscopy characterizations from the Franceschi Microscopy & Imaging Center at Washington State University. Computational resources were provided in part by the Extreme Science and Engineering Discovery Environment (XSEDE) under grant no. MCB170012.

Conflict of Interest

The authors declare no conflict of interest.

Keywords

biopolymers, gelatin, lithium–sulfur batteries, molecular structures, zein

Received: November 5, 2019
Revised: January 12, 2020
Published online: January 31, 2020

[1] a) X. Liu, J. Q. Huang, Q. Zhang, L. Mai, *Adv. Mater.* **2017**, *29*, 1601759; b) Y. C. Jeong, J. H. Kim, S. Nam, R. P. Chong, S. J. Yang, *Adv. Funct. Mater.* **2018**, *28*, 1707411.
[2] R. Xu, J. Lu, K. Amine, *Adv. Energy Mater.* **2015**, *5*, 1500408.
[3] A. Manthiram, S. H. Chung, C. Zu, *Adv. Mater.* **2015**, *27*, 1980.
[4] Z. A. Ghazi, X. He, A. M. Khattak, N. A. Khan, B. Liang, A. Iqbal, J. Wang, H. Sin, L. Li, Z. Tang, *Adv. Mater.* **2017**, *29*, 1606817.
[5] Y. Zhang, R. Wang, W. Tang, L. Zhan, S. Zhao, Q. Kang, Y. L. Wang, S. Yang, *J. Mater. Chem. A* **2018**, *6*, 20926.
[6] G. Hu, C. Xu, Z. Sun, S. Wang, H. M. Cheng, F. Li, W. Ren, *Adv. Mater.* **2016**, *28*, 1603.
[7] L.-X. Miao, W.-K. Wang, A.-B. Wang, K.-G. Yuan, Y.-S. Yang, *J. Mater. Chem. A* **2013**, *1*, 11659.
[8] Y. Li, W. Wang, X. Liu, E. Mao, M. Wang, G. Li, L. Fu, Z. Li, A. Y. S. Eng, Z. W. Seh, Y. Sun, *Energy Storage Mater.* **2019**, *23*, 261.
[9] Z. W. Seh, W. Li, J. J. Cha, G. Zheng, Y. Yang, M. T. McDowell, P.-C. Hsu, Y. Cui, *Nat. Commun.* **2013**, *4*, 1331.
[10] X. Liang, C. Hart, Q. Pang, A. Garsuch, T. Weiss, L. F. Nazar, *Nat. Commun.* **2015**, *6*, 5682.
[11] X. Tao, J. Wang, C. Liu, H. Wang, H. Yao, G. Zheng, Z. W. Seh, Q. Cai, W. Li, G. Zhou, *Nat. Commun.* **2016**, *7*, 11203.
[12] L. Luo, S.-H. Chung, A. Manthiram, *J. Mater. Chem. A* **2016**, *4*, 16805.
[13] J. H. Kim, J. Seo, J. Choi, D. Shin, M. Carter, Y. Jeon, C. Wang, L. Hu, U. Paik, *ACS Appl. Mater. Interfaces* **2016**, *8*, 20092.
[14] E. Peled, I. Shekhtman, T. Mukra, M. Goor, I. Belenkaya, D. Golodnitsky, *J. Electrochem. Soc.* **2018**, *165*, A6051.
[15] L. Li, X. Liu, K. Zhu, J. Tian, X. Liu, K. Yang, Z. Shan, *J. Solid State Electrochem.* **2015**, *19*, 3373.
[16] E. Peled, M. Goor, I. Schektman, T. Mukra, Y. Shoval, D. Golodnitsky, *J. Electrochem. Soc.* **2017**, *164*, A5001.
[17] T. Nakazawa, A. Ikoma, R. Kido, K. Ueno, K. Dokko, M. Watanabe, *J. Power Sources* **2016**, *307*, 746.
[18] N. Akhtar, H. Shao, F. Ai, Y. Guan, Q. Peng, H. Zhang, W. Wang, A. Wang, B. Jiang, Y. Huang, *Electrochim. Acta* **2018**, *282*, 758.
[19] X. Fu, W. H. Zhong, *Adv. Energy Mater.* **2019**, *9*, 1901774.
[20] W.-G. Lim, C. Jo, J. Lee, D. S. Hwang, *Korean J. Chem. Eng.* **2018**, *35*, 579.
[21] X. Fu, C. Li, Y. Wang, L. Scudiero, J. Liu, W. H. Zhong, *J. Phys. Chem. Lett.* **2018**, *9*, 2450.
[22] Q. Qi, X. Lv, W. Lv, Q.-H. Yang, *J. Energy Chem.* **2019**, *39*, 88.
[23] M. Chen, X. Fu, N. D. Taylor, Z. Chen, W.-H. Zhong, *ACS Sustainable Chem. Eng.* **2019**, *7*, 15267.
[24] M. Zhu, Y. Wang, L. Long, X. Fu, G. Sui, X. Yang, *Chem. Eng. J.* **2019**, *370*, 1068.
[25] S. Tu, X. Chen, X. Zhao, M. Cheng, P. Xiong, Y. He, Q. Zhang, Y. Xu, *Adv. Mater.* **2018**, *30*, 1804581.
[26] a) H. M. Kim, H.-H. Sun, I. Belharouak, A. Manthiram, Y.-K. Sun, *ACS Energy Lett.* **2016**, *1*, 136; b) Y. Chen, N. Liu, H. Shao, W. Wang, M. Gao, C. Li, H. Zhang, A. Wang, Y. Huang, *J. Mater. Chem. A* **2015**, *3*, 15235.
[27] a) J. Sun, Y. Huang, W. Wang, Z. Yu, A. Wang, K. Yuan, *Electrochem. Commun.* **2008**, *10*, 930; b) J. Sun, Y. Huang, W. Wang, Z. Yu, A. Wang, K. Yuan, *Electrochim. Acta* **2008**, *53*, 7084; c) H. Shao, C. Li, N. Liu, W. Wang, H. Zhang, X. Zhao, Y. Huang, *RSC Adv.* **2015**, *5*, 47757.
[28] X. Fu, L. Scudiero, W.-H. Zhong, *J. Mater. Chem. A* **2019**, *7*, 1835.
[29] T. Qiu, H. Shao, W. Wang, H. Zhang, A. Wang, Z. Feng, Y. Huang, *RSC Adv.* **2016**, *6*, 102626.
[30] G. Li, M. Ling, Y. Ye, Z. Li, J. Guo, Y. Yao, J. Zhu, Z. Lin, S. Zhang, *Adv. Energy Mater.* **2015**, *5*, 1500878.
[31] Q. Li, H. Yang, L. Xie, J. Yang, Y. Nuli, J. Wang, *Chem. Commun.* **2016**, *52*, 13479.
[32] J. Liu, D. G. Galpaya, L. Yan, M. Sun, Z. Lin, C. Yan, C. Liang, S. Zhang, *Energy Environ. Sci.* **2017**, *10*, 750.
[33] a) W. Bao, Z. Zhang, Y. Gan, X. Wang, J. Lia, *J. Energy Chem.* **2013**, *22*, 790; b) W. Ni, J. Cheng, X. Li, Q. Guan, G. Qu, Z. Wang, B. Wang, *RSC Adv.* **2016**, *6*, 9320.
[34] J. Wang, Z. Yao, C. W. Monroe, J. Yang, Y. Nuli, *Adv. Funct. Mater.* **2013**, *23*, 1194.
[35] M. He, L.-X. Yuan, W.-X. Zhang, X.-L. Hu, Y.-H. Huang, *J. Phys. Chem. C* **2011**, *115*, 15703.
[36] J. D. Schiffman, C. L. Schauer, *Polymer Reviews* **2008**, *48*, 317.
[37] a) R. K. Scopes, *Protein Purification: Principles and Practice*, Springer Science & Business Media, New York **1982**; b) A. Eyler, T. Liu, L. Scudiero, P. C. Wo, W. H. Zhong, *J. Compos. Biodegrad. Polym.* **2015**, *3*, 33.
[38] A. Gennadios, A. H. Brandenburg, C. L. Weller, R. F. Testin, *J. Agric. Food Chem.* **1993**, *41*, 1835.

[39] P. Held, *B.-T. Instruments, Winooski, VT* **2003**.
[40] R. Nagai, N. Taniguchi, *Medical Biochemistry E-Book*, Saunders Elsevier, Edinburgh **2018**, p. 7.
[41] G. Zheng, Q. Zhang, J. J. Cha, Y. Yang, W. Li, Z. W. Seh, Y. Cui, *Nano Lett.* **2013**, *13*, 1265.
[42] a) J. Y. Ji, B. Lively, W. H. Zhong, *Mater. Express* **2012**, *2*, 76; b) M. Nabeta, M. Sano, *Langmuir* **2005**, *21*, 1706.
[43] X. Fu, Y. Wang, L. Scudiero, W.-H. Zhong, *Energy Storage Mater.* **2018**, *15*, 447.
[44] X. Fu, Y. Wang, X. Fan, L. Scudiero, W.-H. Zhong, *Small* **2018**, *14*, 1803564.
[45] Z. W. Seh, Y. Sun, Q. Zhang, Y. Cui, *Chem. Soc. Rev.* **2016**, *45*, 5605.
[46] N. A. Canas, K. Hirose, B. Pascucci, N. Wagner, K. A. Friedrich, R. Hiesgen, *Electrochim. Acta* **2013**, *97*, 42.
[47] C. Barchasz, J.-C. Leprêtre, F. Alloin, S. Patoux, *J. Power Sources* **2012**, *199*, 322.
[48] X. Zhao, H. Zhu, B. Zhang, J. Chen, Q. Ao, X. Wang, *Journal of the American Oil Chemists' Society* **2015**, *92*, 975.